OPEN

Clinoptilolite in Dextran Sulphate Sodium-Induced Murine Colitis: Efficacy and Safety of a Microparticulate Preparation

*Stéphane Nizet, PhD,[*] Eduardo Muñoz, MD,[†] Bernd L. Fiebich, PhD,[‡] Peter M. Abuja, PhD,[§] Karl Kashofer, PhD,[§] Kurt Zatloukal, MD,[§] Simone Tangermann, DVM,[††] Lukas Kenner, MD,[¶,**,††] Cornelius Tschegg, Dr.[*] Dietmar Nagl, Mag.,[*] Laurenz Scheichl, DI,[*] Claudia Meisslitzer-Ruppitsch, Dr.,[*] Michael Freissmuth, MD,[‡‡] and Thomas Berger, Dr.[*]*

Background: Clinoptilolite is an aluminium silicate of natural origin; the microporous structure and the net negative charge of its crystal lattice allows for adsorption of ions, toxins, inflammatory mediators, and some microorganisms. We generated 2 preparations of purified clinoptilolite, which differed by about 10-fold in particle size, ie, a standard powder (GHC1) and a microparticulate fraction (GHC2) with a size of 3.6 µm and 0.39 µm (d_{50}) respectively. These were examined for their ability to accelerate the recovery of mice from DSS (dextran sulphate sodium)-induced intestinal inflammation.

Methods: Efficacy of clinoptilolite preparations was investigated by administering DSS-treated mice twice daily with 30 mg GHC2 or GHC1 for 5 consecutive days, followed by 5 days of recovery without DSS. To explore the safety of the microparticulate preparation (GHC2), mice were subjected to 4 cycles of DSS-exposure. We specifically verified that clinoptilolite microparticles were not systemically bioavailable by examining the gut tissue and the liver for the accumulation of microparticles by transmission electron microscopy.

Results: Treatment of mice with GHC2 was superior to GHC1 and as effective as the reference compound 5-aminosalicylic acid in ameliorating the damage induced by the exposure to DSS. In addition, no clinoptilolite particle was observed in the intestinal epithelial layer, gut-associated lymph follicles, or in the liver.

Conclusion: Our observations confirm that a microparticulate preparation of clinoptilolite is safe and effective in a murine model of inflammatory bowel disease and supports the hypothesis that the adsorptive capacity of clinoptilolite is of potential therapeutic relevance.

Key Words: colitis, DSS, zeolite, inflammation

Clinoptilolite is a natural zeolite mineral consisting of hydrated (Ca, Na, K, and Mg) aluminium silicate. Due to its porous structure and the net negative charge of its crystal lattice, clinoptilolite has a high adsorptive capacity and can act as a cation exchanger. Accordingly, clinoptilolite binds heavy metals.[1–3] Administration of micronized clinoptilolite limits the bioavailability of ingested lead and of other heavy metals.[4] Clinoptilolite and related clays have been widely used in animal husbandry; when admixed to the animal feed, clinoptilolite promotes animal weight gain.[5,6] The underlying mechanism is not clear, but its beneficial actions may arise from its ability to preclude the absorption of mycotoxins[6–8] and to reduce the presence of potentially pathogenic bacteria in the gut of treated animals.[9] At the very least, the widespread use of clinoptilolite in farm animals suggests that it can be safely administered by the oral route.[10,11] In addition, clinoptilolite also is innocuous when instilled into the lung.[12]

Exaggerated claims are rampant in the field of clinoptilolites, such as a remedy for many different disorders including immunodeficiencies[13] and various cancers.[14] Marketing it as a panacea in alternative and complementary medicine also is not establishing a scientifically sound approach to exploring its therapeutic potential and its mechanism of action. However, randomized control trials showed that the administration of clinoptilolite and related clays reduces the incidence of and accelerates the recovery from scour (porcine endemic diarrhea) in weaning piglets[15] and protects newborn calves against diarrhea.[16]

Received for publication July 10, 2017; Editorial decision October 6, 2017.

*GLOCK Health, Science and Research GmbH, Deutsch-Wagram, Austria; [†]Maimonides Biomedical Research Institute of Córdoba, Reina Sofía University Hospital, Department of Cell Biology, Physiology and Immunology, University of Córdoba, Córdoba, Spain; [‡]VivaCell Biotechnology GmbH, Denzlingen, Germany; [§]Institute of Pathology, Medical University of Graz, Graz, Austria; [¶]Department of Experimental and Laboratory Animal Pathology, Medical University of Vienna, Austria; [**]Ludwig Boltzmann Institute for Cancer Research (LBI-CR), Vienna, Austria; [††]Unit of Laboratory Animal Pathology, University of Veterinary Medicine Vienna, Vienna, Austria; [‡‡]Institute of Pharmacology & Gaston H. Glock Research Laboratories for Exploratory Drug Development, Center for Physiology and Pharmacology, Medical University Vienna, Vienna, Austria

Conflicts of Interest: Stéphane Nizet, Dietmar Nagl, Laurenz Scheichl, Claudia Meisslitzer-Ruppitsch, Cornelius Tschegg and Thomas Berger are employees of Glock Health, Science and Research GmbH, a company developing clinoptilolite-based medicine products. The company owns a patent based on the clinoptilolite powder used in this work (US patent 2015/0132387). The other authors have no conflicts of interest to declare.

Address correspondence to: GLOCK Health, Science and Research G.m.b.H., Hausfeldstraße 17, A-2232 Deutsch-Wagram, Austria. E-mail: stephane.nizet@glock.at

doi: 10.1093/ibd/izx042
Published online 19 December 2017

These findings suggest that the adsorptive capacity of clinoptilolite is useful to reduce gut inflammation and to promote the recovery of the damaged epithelium. Accordingly, these findings on clinoptilolite also may represent a therapeutic option in the treatment of human inflammatory bowel diseases (IBDs).

The 2 most prevalent human chronic IBDs are ulcerative colitis (UC) and Crohn's Disease (CD); their incidence has been rising in the industrialized countries over the past 50 years.[17,18] The causative agents are poorly understood but it is clear that environmental (microbiome, hygiene, plant fibers, vitamin D, etc.) and genetic factors interact to drive the emergence and the progression of chronic intestinal inflammation: in fact, over 200 human gene loci have been identified that are associated with an increased susceptibility to IBDs.[19,20] Some aspects of the underlying pathophysiology can be recapitulated in animal models of intestinal inflammation. Here, we examined the hypothesis that the adsorptive actions of clinoptilolite are useful to promote recovery of the intestinal epithelium in a murine model of IBD triggered by the administration of dextran sulphate sodium (DSS).[21] Our experiments were designed to obtain evidence for efficacy by comparing 2 preparations of micronized clinoptilolite that differ in average particle size and, hence, in surface area. As posited working hypothesis, the microparticulate clinoptilolite preparation (GHC2) is assumed to be more efficacious because of its larger surface. This conjecture was first confirmed in an acute murine colitis model, which showed that the administration of microparticulate clinoptilolite was as effective as that of the reference compound 5-aminosalicylic acid in promoting the recovery from intestinal inflammation. In addition, we subsequently verified the safety of this microparticulate fraction by prolonged administration to animals with a sustained DDS-induced intestinal inflammation.

MATERIALS AND METHODS

Unless indicated otherwise, chemicals were of analytical grade and were purchased from Sigma-Aldrich (St. Louis, MO, USA).

Preparation and Characterisation of Clinoptilolite

The raw material (clinoptilolite-tuff) originates from the mining site Nizny Hrabovec in the Slovak Republic. After extraction from the mine, the raw material was coarsely crushed to select solely pieces containing no postvolcanogenic Mn/Fe-oxide crusts for further purification steps. The clean raw material underwent detailed quality inspections before it was subsequently released to a validated high quality controlled and well-documented refining process. After the mechanical conditioning steps, the naturally bound heavy metals in the raw material were depleted through a patented process (US patent number 8173101). Finally, the purified clinoptilolite was micronized (d_{50} = 3.6 µm) and subjected to dry heat for 2 hours at 160°C. Its particle size distribution was measured by laser diffraction analysis (Mastersizer 2000, Malvern Instruments, England). The final product was defined as standard clinoptilolite (referred to as GHC1). To prepare the microparticulate clinoptilolite (=GHC2), a suspension of GHC1 particles in water at a concentration of 10% (wt/vol) was centrifuged for 10 minutes at 200*g*. The supernatant, containing particles smaller than 1 µm, was collected and concentrated by centrifugation for 30 minutes at 3000*g*. The chemical composition of clinoptilolite samples was determined after microwave-assisted hydrofluoric acid pressure digestion in a Multiwave 3000 (Anton Paar GmbH; Graz, Austria) by inductively coupled plasma-mass spectrometry/ICP-MS (Elan DRC-e; Perkin Elmer, USA). Beyond those methods, the mineralogical composition of the material used in the study was confirmed and controlled via X-ray diffraction (Bruker D8 Venture, Bruker, USA).

Sample preparation of clinoptilolite particles for scanning electron microscopy

Particles of clinoptilolite were suspended in water at a concentration of 100 mg/ml and treated in an ultrasonic bath for 10 seconds (Sonorex RK 52 H, Bandelin, Germany). The suspension was further diluted to 1:100 (vol/vol) with methanol and ultra-sonicated for another 10 seconds. Nucleopore filter membranes with a pore size of 0.1 µm were placed into centrifugal filter units (VWR; Vienna, Austria). Methanol (193 µl) and the clinoptilolite suspension (7 µl) were mixed, pipetted onto the filter, and centrifuged for 2 minutes at 5000*g*. The filters were then mounted on carbon adhesive tabs (Science Services; Munich, Germany) placed on aluminium pins (Science Services, Germany).

All samples were dried under ambient conditions, sputter-coated with gold (Cressington Sputter Coater 108 auto, Cressington Scientific Instruments Ltd., Watford, UK) and analyzed with a Tescan Vega Series Scanning Electron Microscope (Tescan, Brno; Czech Republic) operated at 15.0 kV.

DSS-induced Acute and Chronic Colitis

In the acute colitis model, male Swiss-Webster mice, aged between 10–14 weeks, were purchased from Harland Laboratories (NL) and housed in the animal facilities of the University of Córdoba (Córdoba, Spain) under controlled conditions (12 hour light/dark cycle; temperature 20 ± 2°C, and 40–50% relative humidity) with ad libitum access to standard food and water. The experiment was performed in strict adherence to the European Union guidelines and approved by the Animal Research Ethic Committee of the Córdoba University (2015PI/07). Twelve mice each were randomly assigned to the experimental groups. DSS (3% wt/vol in water; dextran sulphate sodium (DSS) Mt = 40 kDa, Sigma-Aldrich, Spain) was administered in the drinking water for 5 consecutive days (day 0 to 5). As a consequence, the animals developed the characteristics of colitis, ie, loose stools and diarrhea, anal mucus, and

weight loss. From day 6 onwards, mice received by oral gavage either 5-aminosalicylic acid (5-ASA, mesalazine-positive control; 300 µL, 150 mg/kg, in water), water alone (DSS; 300 µl), standard clinoptilolite (GHC1, 30 mg/300 µl), or microparticulate clinoptilolite (GHC2, 30 mg/300 µl) twice daily with an interval of 12 hours. Control mice remained untreated during the whole duration of the study. On day 10, the mice were killed by cervical dislocation, the colon was dissected, and prepared for subsequent analysis by the Swiss roll technique. Aliquots of the samples were snap-frozen and stored at -80°C.

For chronic DSS-induced colitis male and female C57BL/6J mice (10–14 weeks of age) were obtained from Charles River (Germany). Animals were kept in a specific pathogen-free facility at the Medical University of Graz, Austria, at controlled temperature (25 ± 1°C) and humidity (50–65% relative humidity) on a 12 hour day/night cycle. This animal experiment was approved by the Austrian Ministry of Science, Research and Economy (GZ.: BMWFW-66.010/0108-WF/II/3b/2014), and animal suffering was kept to a minimum. The chow was prepared by Ssniff (Soest; Germany) by mixing standard chow with 10% (wt/vol) of microparticulate clinoptilolite (GHC2) suspension in ultrapure water at a concentration of 20% (wt/vol), yielding a final concentration of 2% clinoptilolite in chow. Control animals received standard chow (Ssniff) with 8% admixed tap water to account for the addition of water in the treatment. The chow was sterilized by γ-irradiation (25 kGy) and stored at room temperature until use. Mice were randomly allocated to 3 groups of 10 male and 10 female mice: the first group was designated as control group and received no treatment. The second and the third groups were exposed to DSS in drinking water to induce colitis: the animals received DSS (2% in the drinking water, which was provided ad libitum) every other week, starting with the second week, ie, in weeks 2, 4, and 6. In week 8, animals received 3% DSS in the drinking water. The first (=control group) and the second group (DSS-treated group) received regular chow, which had been supplemented with 8% water to match the water content of the experimental diet. The third group was fed with chow supplemented with 2% clinoptilolite and 8% water. The animals were killed after 9 weeks: mice were anesthetized with 2% isoflurane and killed by exsanguination via heart puncture. Organs (caecum, colon, spleen, liver, kidney, and brain) were removed. Colon length was measured before it was opened lengthwise, the colon content was sampled, and the colon mucosa carefully rinsed with ice-cold PBS (Phosphate Bufferered Saline) to remove most of the attached luminal content (stool and clinoptilolite). The tissue was fixed in formalin and subsequently embedded in paraffin for histopathological examination or fixed for electron microscopy (see below—Tissue Histopathology).

Real-time PCR

Total RNA was isolated from the distal colon tissue using the RNAeasy Mini Kit (Qiagen, Germany) according to the instructions of the manufacturer. One µg of RNA was retrotranscribed using the iScriptTM cDNA Synthesis Kit (Bio-Rad, Hercules, CA, USA), and the cDNA was analyzed by real-time PCR, using the iQTM SYBR Green Supermix (Bio-Rad, Germany). Real-time PCR was performed using a CFX96 Real-Time PCR Detection System (Bio-Rad, Germany). Primers for interleukin-1β (IL-1β), interleukin-6 (IL-6), tumour necrosis factor-α (TNF-α), and GAPDH were used (see Supplemental Digital Content 1, SDC1, which lists the respective forward and reverse primers).

Primer efficiency was verified by serial dilutions. The GAPDH housekeeping gene was used to standardize the mRNA expression levels in each sample. The amplification of GAPDH required about 20 cycles to reach the detection threshold; this number was subtracted from the cycle threshold for the amplification of the 3 cytokines.

Tissue Histopathology

Tissues were fixed in buffered formalin (4% formaldehyde in 10 mM phosphate buffer, pH 6.8; Sigma-Aldrich, Austria), processed, and embedded in paraffin. Sections (5 µm thick) were stained with hematoxylin and eosin (H&E; Sigma-Aldrich, Austria) and coded. The histopathological evaluation was performed by board-certified pathologists (Simone Tangermann, Lukas Kenner) in a blinded fashion. A scoring system was established based on 5 histological parameters to quantify the extent and severity of tissue damage: (i) destruction of epithelium and glands (0 = normal, 1 = focal destruction of epithelial surface and/or crypts, 2 = zonal destruction of epithelium surface and/or crypts, and 3 = wide ulcerations that involve mucosa and submucosa). (ii) dilation of glandular crypts (0 = normal, 1 = focal dilation, 2 = zonal dilation, and 3 = wide dilation). (iii) depletion or loss of goblet cells (0 = no depletion, 1 = slight loss, 2 = mild loss, and 3 = wide loss). (iv) infiltration of inflammatory cells (0 = no infiltration, 1 = subepithelial infiltration at the level of lamina propria, 2 = infiltration extending to lamina muscularis mucosae, and 3 = wide infiltration that involves submucosa). (v) inflammatory cell distribution (0 = normal, 1 = mild inflammation, 2 = more widely distributed inflammation, and 3 = extensively widely distributed inflammation). The histological score corresponds to the sum of the points assigned to each individual parameter. The maximum possible score was 15.

Transmission Electron Microscopy

Organs were fixed in 2.5% glutaraldehyde/4% formaldehyde in Tris-HCl (10 mM, pH = 7.4, VWR, Austria) and stored at 4°C until further treatment. Samples were postfixed for 20 minutes at room temperature with 1% osmium tetroxide in water (Science Services, Germany). Dehydration in a graded ethanol series (0-30-50-70-90-95-100%, VWR, Austria) was followed by a stepwise embedding in epoxy resin (EMbed-812 Kit, Electron Microscopy Sciences, USA). Polymerization was performed at 60°C for 2 days in beem capsules (easy-molds,

Electron Microscopy Sciences, USA). Semithin sections were cut with an EM UC6 ultramicrotome (Leica Microsystems, Vienna, Austria) and stained with 0.5% Azur II and 1% methylene blue in 1% sodium borate (Sigma-Aldrich, Austria). Ultrathin sections were transferred to copper grids (Science Services, Germany) and stained for 15 minutes in uranyl acetate (Science Services, Germany) and for 5 minutes in lead citrate (Science Services, Germany), each at room temperature. Grids were analyzed with a Tecnai twin G20 transmission electron microscope (FEI Company, Eindhoven, The Netherlands) equipped with a LaB6 cathode and operated at 120 kV.

Microbiome Analysis

Colon contents were sampled after killing directly from the colon/rectum (1–2 most distal pellets) and stored at -80°C until analysis. DNA was extracted from stool samples following the recommended procedures using the Magnapure Bacterial DNA Kit (Roche, Austria) and a Hamilton Starlet workstation (Hamilton Robotics, Bonadur, Switzerland). DNA concentration was measured by PicoGreen fluorescence (Thermo Fisher Scientific, Waltham, MA, USA). The variable V1–V2 region of the bacterial 16S rRNA gene was amplified by PCR from DNA (50 ng) using oligonucleotide primers 16S_515_S3_fwd: GATTGCCAGCAGCCGCGGTAA and 16S_806_S2_rev: GGACTACCAGGGTATCTAAT. This 16S rDNA region was chosen because it gives robust taxonomic classification and has been shown to be suitable for community clustering.[22] Bacterial 16S rRNA was amplified with the Mastermix 16S Complete PCR Kit (Molzym, Bremen, Germany). The first PCR product was subjected to a second round of PCR with primers fusing the 16S primer sequence to the A and P adapters necessary for Ion Torrent sequencing while additionally including a molecular barcode sequence to allow multiplexing of up to 96 samples simultaneously. PCR products were subjected to agarose gel electrophoresis and the band of the expected length (330 nt) was excised from the gel and purified using the QiaQuick gel extraction system (Qiagen, Hilden, Germany). DNA concentration of the final PCR product was measured by PicoGreen fluorescence. Equimolar amounts of amplicons were pooled from up to 60 samples and subjected to emulsion PCR using the Ion Torrent One Touch 2.0 Kit according to manufacturer's protocols. After emulsion PCR, the beads were purified on the Ion ES station and loaded onto Ion Torrent 318 chips for sequencing. Sequencing reactions were performed on the Ion Torrent PGM using the Ion 400BP Sequencing Kit running for 1,082 flows (all reagents from ThermoFisher Scientific, MA, USA). Sequences were split by barcode and transferred to the Torrent suite server. Unmapped BAM files were used as input for bioinformatics analyses. All sequences were initially trimmed by a sliding window quality filter with a width of 20 nt and a cutoff of Q20. Reads shorter than 100 nucleotides and reads mapping to the human genome were removed using the DeconSeq tool.[23] The resulting reads were subjected to error correction using the Acacia tool,[24] leading to error correction in 10–20% of reads. Subsequently PCR chimeras were removed by usearch algorithm in de novo and reference-based settings.[25] The final sequence files were then analyzed by QIIME 1.8 workflow scripts.[26] OTU (operational taxonomic unit) search was performed using the parallel_pick_open_reference_otus workflow script and the greengenes 13_8 reference database (http://qiime.org/scripts/pick_open_reference_otus.html). OTUs were visualized as OTU tables, bar charts, and PCoA (principal component analysis) plots using the QIIME core microbiome script. Additionally, groupings supplied in the mapping file were tested for statistical significance using the QIIME implementation of the Adonis test and significance of individual bacterial strains was determined by Kruskal-Wallis test. LEfSe analysis[27] was performed to detect statistically relevant strains in several of the study groups.

RESULTS

Two Clinoptilolite Preparations Differed in Particle Size but Had an Identical Chemical and Mineralogical Composition

Clinoptilolite minerals can be contaminated with trace amounts of toxic alkaline earth metals (eg, barium), heavy metals (eg, lead, mercury), and/or arsenic. These contaminants can be depleted from clinoptilolite by ion exchange procedures. We characterized the final preparations, which were produced by ion exchange followed by micronizing to generate a coarse-grained (GHC1), and an additional centrifugation step to produce a microparticulate (GHC2) preparation. The morphology and the surface characteristics of clinoptilolite particles were inspected using a scanning electron microscope whereas the size was measured by laser diffraction analysis. With the exception of the size, both powders were indistinguishable (Fig. 1).

The particle size distribution of the two clinoptilolite preparations is shown in Table 1. In the standard clinoptilolite powder (GHC1), 90% of the population of particles were below 6.7 µm, 10% were below 1.5 µm, and the median size was at 3.56 µm. In contrast, the microparticulate preparation (GHC2) was composed predominantly of particles of a median size of 0.34–0.39 µm, which were averaging about 1 10th in size of the standard powder (GHC1) with 90% of the particles smaller than 1 µm.

The chemical composition of the standard powder (GHC1) is summarized in Table 2. The bulk of the material was identified as aluminium silicate with cations (ie, Na^+, K^+, Mg^{2+}, and Ca^{2+}) trapped in it. Ion exchange resulted in the depletion of toxic metals and metalloids: accordingly, the final levels of lead, barium, manganese, and arsenic were 2.23 ± 0.02, 57.9 ± 0.3, 13.9 ± 0.2, and 0.65 ± 0.03 µg/g, respectively. The mineralogical and chemical compositions of standard (GHC1) and microparticulate clinoptilolite (GHC2) were comparable to each other.

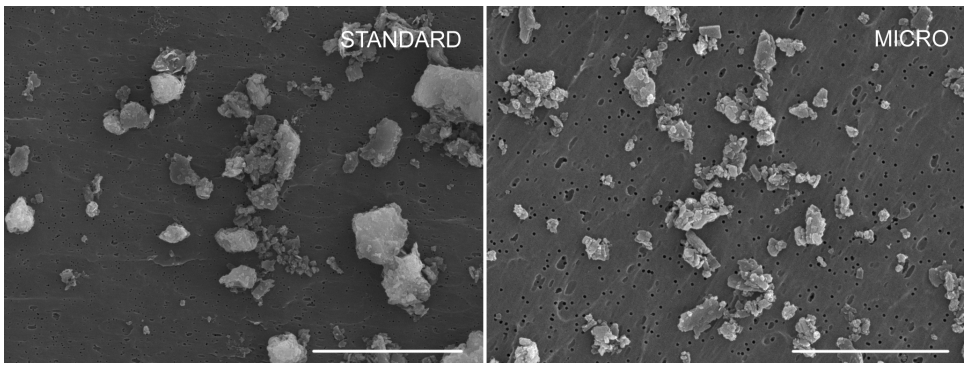

FIGURE 1. Scanning electron microscopic view of powdered standard (GHC1, left hand image) and microparticulate (GHC2, right hand image) clinoptilolite. Samples were prepared as outlined under Materials and Methods, coated with gold, and imaged under a Tescan Vega Series Scanning Electron Microscope at a magnification of 4910-fold (left hand image) and 18,760-fold (right hand image). The scale bars correspond to 20 µm and 5 µm in the left and right hand images, respectively.

Microparticulate Clinoptilolite Preparation Mitigated Intestinal Inflammation in an Acute Colitis DSS Mouse Model

Several bacterial species are adsorbed by clinoptilolite and other zeolites.[28,29] We confirmed that our clinoptilolite preparation bound several bacterial species, mycotoxins, and inflammatory mediators in vitro: see Supplemental Digital Content 2 (SDC2) and Supplemental Digital Content 3 (SDC3), which show—as representative examples—the adsorption of *Enterococcus cloacae* and of TNF-α, respectively, to microparticulate clinoptilolite (GHC2). A factor, which contributes to the pathophysiology of IBD, is the enhanced permeability of the epithelial barrier, which allows for the leakage of bacterial fragments.[30–32] The enhanced permeability can be recapitulated by the administration of DSS in mice.[33,34] Prolonged administration of clinoptilolite to human subjects induces changes in surrogate markers indicative of an improved epithelial barrier.[35] Accordingly, we explored the possibility that the administration of clinoptilolite mitigates the course of DSS-induced bowel inflammation. After 5 days of exposure to 3% DSS in the drinking water, all mice experienced diarrhea and weight loss (by about 1 g). The animals were subsequently treated twice daily by oral gavage with standard (GHC1) or microparticulate clinoptilolite (GHC2) at a dose of 30 mg/300 µl. Healthy mice served as control and showed an intact histology (Fig. 2A). In the DSS group, which received only vehicle (=300 µl water) by gavage, the damage was most extensive: ulcerations of the mucosa and submucosa were present and the infiltration of inflammatory cells extended in most of the samples to the submucosa (Fig. 2B) resulting in an average score of 9 (Fig. 2C). In mice exposed to DSS and subsequently treated with standard powdered clinoptilolite (GHC1), the histological lesions were comparable (Fig. 2D) to those seen in animals solely exposed to DSS. Accordingly, the mean histological score (8.75) was similar in magnitude (Fig. 2C). In mice, which were administered DSS and the microparticulate powered clinoptilolite GHC2, the histological lesions were milder: ulcerations of the epithelium were only seen occasionally and inflammatory cells were rarely present in the submucosa (Fig. 2E). Accordingly, the histological damage score was significantly improved, when compared to both, DSS- and DSS+GHC1-treated animals. In fact, the beneficial action of GHC2 was comparable to that achieved by 5-aminosalicylic acid (ASA), which was used as reference treatment (Fig. 2F). Consequently, the histological scores were comparable in GHC2- and 5-aminosalicylic acid-treated animals (Fig. 2C).

Decreased inflammation was also seen in the expression profile of proinflammatory cytokines assessed by RT-PCR. Exposure of animals to DSS resulted in elevated levels of transcripts (reduced cycle thresholds ΔC_t in Fig. 3) for interleukin-1β (IL-1β, Fig. 3A), interleukin-6 (IL-6, Fig. 3B), and tumour necrosis factor-α (TNF-α, Fig. 3C) in the gut tissue. The levels of IL-1β (Fig. 3A) and IL-6 (Fig. 3B) transcripts were reduced in a statistically significant manner by treatment of mice with both the standard (GHC1) and the microparticulate (GHC2) preparations of clinoptilolite and by administration of 5-aminosalicylic acid, but GHC2 was superior to GHC1: administration of GHC2 caused a significantly larger reduction in IL-6 transcript levels than GHC1 (Fig. 3B). In contrast, the levels of TNF-α were not affected by any treatment regimen (Fig. 3C).

Microparticulate Clinoptilolite Fraction Was Well Tolerated in a Murine Chronic Colitis DSS Model

Taken together, the experiments summarized in Figures 2 and 3 showed that clinoptilolite had some beneficial action in DSS-induced colitis. The efficacy of the microparticulate preparation (GHC2) was more pronounced than that of GHC1 such that not only did it mitigate biochemical markers of inflammation but also it affected epithelial damage quantifyably. GHC2, however, is composed of very small particles. Upon repeated

TABLE 1: Particle Size Distribution of Standard and Microparticulate Clinoptilolite

Mean diameter	d_{10} µm	d_{50} µm	d_{90} µm
Standard clinoptilolite GHC1	1.48 ± 0.02	3.56 ± 0.05	6.70 ± 0.11
Microparticulate clinoptilolite GHC2 (acute DSS-model)	0.19 ± 0.00	0.39 ± 0.00	1.09 ± 0.00
Microparticulate clinoptilolite GHC2 (chronic DSS-model)	0.17 ± 0.00	0.34 ± 0.00	1.01 ± 0.00

Clinoptilolite was micronized to generate powdered preparations GHC1 and GHC2 as outlined under Materials and Methods. The size of the particles was determined by Mie scattering in a Malvern Mastersizer 2000; d_{10}, d_{50}, and d_{90} define the diameter under which 10%, 50%, and 90%, respectively, of the volume fraction are found. Diameter is given as median size ± standard deviation (n = 3). The 2 preparations of microparticulate clinoptilolite GHC2 used in the acute and chronic DSS model were characterized independently to verify that they were comparable.

administration, these submicron particles could possibly elicit untoward effects by breaching the epithelial barrier and/or by accumulating in macrophages of Peyer's patches.[36,37] We tested for toxic effects by applying clinoptilolite particles to a monolayer of Caco-2 cells. This human cell line is derived from a colonic adenocarcinoma and, when grown in culture under appropriate conditions, recapitulates key features of the human small intestinal epithelial layer.[38] We neither observed any effect on cell viability nor transepithelial transport of clinoptilolite particles (data not shown). However, the tight epithelial layer of Caco-2 cells in culture is unlikely to recapitulate the leaky lining of the chronically inflamed intestine. We therefore exposed mice to repeated challenges with DSS and treated them chronically with GHC2: the animals were treated for 9 weeks every other week with DSS in their drinking water (ie, for 4 cycles of DSS, see schematic representation in Fig. 4A) and received clinoptilolite via their chow throughout the same period. The resulting chronic inflammation led to a substantial shortening of the colon: as can be seen in Figure 4B, colon length in male and female DSS-treated animals was reduced by 46% and 34%, respectively. Mice that received clinoptilolite were partially protected from DSS-induced colon shortening. The effect was more pronounced in female mice, whereas the difference between mice solely exposed to DSS and those receiving GHC2 in addition was statistically significant (ANOVA followed by Holm-Sidak multiple comparisons, $P = 0.007$). In contrast, in male mice, this difference failed to reach the threshold of statistical significance ($P = 0.10$). We separately verified with a cohort of healthy control mice that the chronic ingestion of clinoptilolite via the fortified chow per se did not affect food intake (data not shown).

Intestinal Layers and Liver of Mice Chronically Exposed to Microparticulate Clinoptilolite Preparation Were Devoid of Particles

Because of the small size of the clinoptilolite particles in GHC2, they could not be readily detected by light microscopy. However, they could be visualized by transmission electron microscopy of ultrathin sections due to the high density of their crystal structure. This is exemplified in Figure 5A. Clinoptilolite particles were readily identified in the intestinal

TABLE 2: Chemical Composition of Standard and Microparticulate Clinoptilolite

	% of Total Mass		
	Standard Clinoptilolite GHC1	Microparticulate Clinoptilolite GHC2 (acute DSS model)	Microparticulate Clinoptilolite GHC2 (Chronic DSS Model)
SiO_2	71.6 ± 5.0	70.5 ± 1.6	71.0 ± 0.7
Al_2O_3	13.4 ± 0.2	12.6 ± 0.1	13.0 ± 0.3
MgO	0.4 ± 0.0	0.5 ± 0.0	0.5 ± 0.0
Na_2O	0.6 ± 0.0	0.1 ± 0.0	0.1 ± 0.0
K_2O	1.3 ± 0.0	2.1 ± 0.0	2.0 ± 0.0
CaO	4.2 ± 0.1	3.5 ± 0.0	3.4 ± 0.1
		Concentration [µg/g]	
As	0.65 ± 0.03	1.33 ± 0.17	2.36 ± 0.12
Ba	57.9 ± 0.3	21.1 ± 1.8	31.7 ± 1.5
Pb	2.23 ± 0.02	1.94 ± 0.15	2.26 ± 0.11

The chemical analysis was done by ICP-MS as outlined under Materials and Methods. Bulk elements (upper part of the table) are given as % of total mass; trace contaminants (lower part of the table) as µg/g. The microparticulate preparations used in the acute and chronic DSS model were characterized independently to verify that they were comparable.

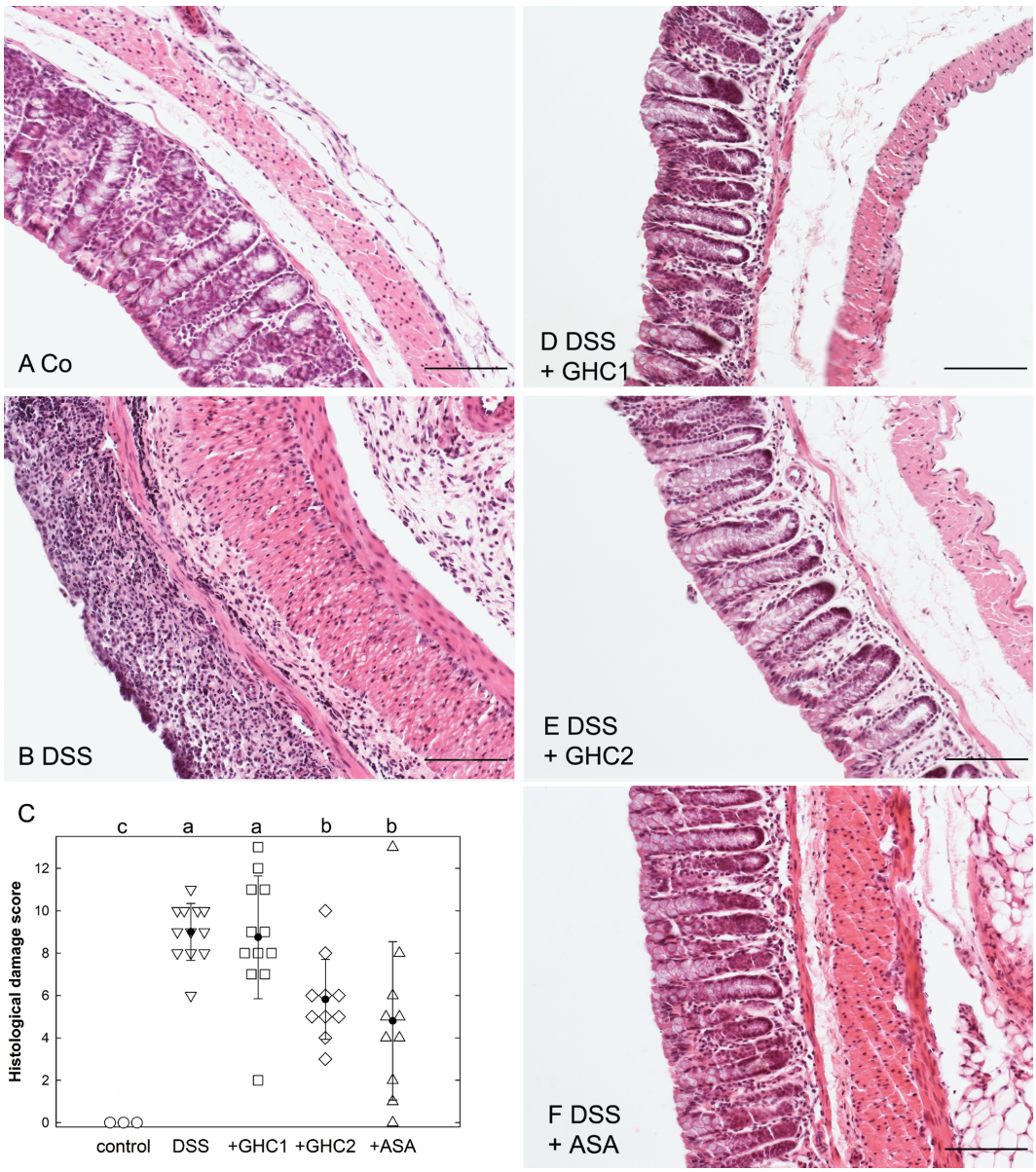

FIGURE 2. Representative images of histological sections through colon specimens from untreated control mice (A), mice exposed to 3% DSS in the drinking water for 5 days (B), mice exposed to 3% DSS and subsequently treated for 5 days with standard powdered clinoptilolite (GHC1; C), with microparticulate clinoptilolite (GHC2; D) or with 5-aminosalicylic acid (ASA; E) and the summary of the histological score (F). Paraffin-embedded sections were stained with hematoxylin and eosin and examined by microscopy to obtain a histological score for each animal (individual values and means ± S.D. are indicated in Panel F) as outlined under Materials and Methods. The DSS group showed extensive damage (B) and an elevated damage score (C). Whereas GHC1 failed to significantly attenuate the inflammation (D), GHC2 showed only mild inflammation (E) and a significantly lower damage score (C). 5-ASA, used as positive control, mitigated the inflammation similar to GHC2 (C and F). Healthy mice, used as control, showed no signs of inflammation (A and C). The statistical comparison was done by ANOVA followed by Tukey's posthoc test, which showed that there was a significant difference between the following groups: GHC2 vs. DSS ($P = 0.025$), GHC2 vs. GHC1 ($P = 0.045$), ASA vs. DSS ($P = 0.0025$) and ASA vs. GHC1 ($P = 0.005$). For all groups with the same letter, the difference between the means was not statistically significant. If 2 groups have different letters, they were significantly different ($P < 0.05$).

lumen. This unequivocally demonstrated that the approach was, in principle, suitable for the detection of clinoptilolite particles in biological samples without the need for specific labeling. Accordingly, we investigated the possibility that clinoptilolite particles cross the gut barrier through uptake by enterocytes or transport in the lymph follicles. For this purpose, the intestines of mice chronically treated with both DSS and GHC2 particles were embedded in epoxy resin and semisectioned until the section plane crossed at least one lymph follicle. Ultrathin sections were prepared, contrasted, and inspected

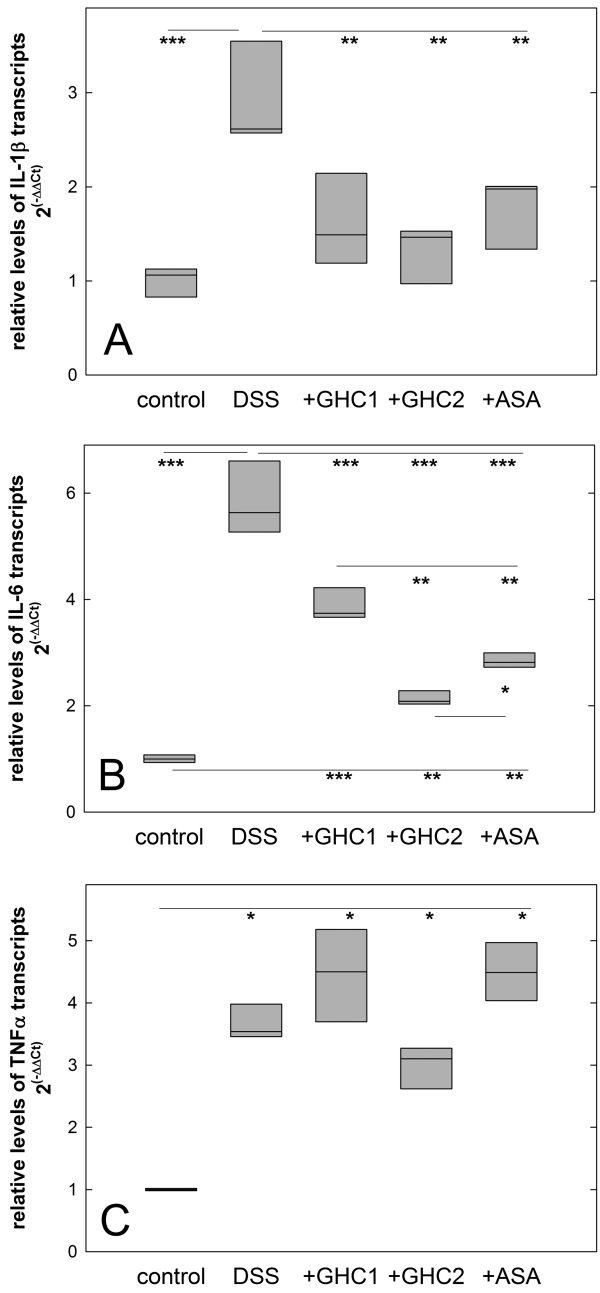

FIGURE 3. Quantification of transcripts for interleukin-1β (IL-1β, A), interleukin-6 (IL-6, B) and tumour necrosis factor-α (TNF-α, C). Total RNA was extracted from the distal colon of the animals used in Figure 2, reverse transcribed and amplified using the primers listed under Materials and Methods. The internal standard was GAPDH, the cycle threshold for GAPDH (about 20 cycles) was subtracted to yield ΔCt-values, which were normalized to the mean of the control animals. Shown are the resulting ΔΔCt-values for each amplicon. Box plots show the median and the interquartile range, whiskers indicate the 95% confidence interval. The statistical comparison was done by ANOVA or by a Kruskal-Wallis test followed by pairwise multiple comparison with the Holm-Sidak procedure or by Dunn's posthoc test (as appropriate): the statistical analysis showed that—when compared to DSS-treated animals—GHC2, GHC1 and 5-aminosalicylic acid (ASA) significantly (*, $P < 0.05$; **, $P < 0.01$; ***, $P < 0.001$) reduced the amplicons of IL-1β (A) and IL-6 (B) but not of TNF-α (C).

by transmission electron microscopy. No clinoptilolite particle was observed in the epithelial layer (not shown). Similarly, no particle was visible in the lymph follicles (Fig. 5B). We stress that 48 sections were examined and we did not detect a single clinoptilolite particle—neither in immune cells nor in the extracellular compartment of the lymph follicles. Interestingly, in the gut lumen, clinoptilolite particles were typically found at some distance from the microvilli covering the epithelium rather than in close contact to the epithelium (Fig. 5A). This indicates that they probably cannot readily penetrate the mucus layer.

If clinoptilolite particles did cross the intestinal barrier, they would either enter the systemic circulation directly via capillaries or indirectly via lymphatic vessels. In either case, the particles ought to be eventually bound to and phagocytosed by Kupffer cells in the liver, because they are too large for renal filtration. Hence, we explored the possibility of clinoptilolite reaching the liver by preparing sections of mouse livers for transmission electron microscopy. Ten ultrathin sections from 10 different livers were examined. None revealed a single clinoptilolite particle (not shown). Taken together, the results indicate a very low probability that clinoptilolite particles cross the intestinal barrier and are distributed systemically.

Administration of Microparticulate Clinoptilolite Preparation Modified Stool Microbiome in Chronic Colitis DSS Mouse Model

PCoA based on the unweighted unifrac distances after 16S-rRNA sequencing revealed a clear separation of the 3 experimental groups (see Fig. 6A showing a plot of the 3 components that contribute most to the group differences). LEfSe analysis calculates the effect size for each OTU and assigns statistical significance via the linear discriminant analysis (LDA) score.[27] Graphical representation of taxonomic units with a significant LDA score in a cladogram (Fig. 6B) showed a clear separation of the 3 treatment groups. The cladogram displays taxonomic groups with significant LDA score from phylum level (innermost circle) down to familia level (outermost circle). The phylum *Deferribacteres* showed a significant LDA score from the phylum level down to the species level establishing an almost exclusive presence of this phylum in the DSS group. Similarly, *Verrucomicrobia* were mostly present in the DSS group. The *Bacteroidetes* phylum was abundant in the control group indicating a reduction of this phylum in both, DSS- and DSS+GHC2-treated animals with only few *Bacteroidetes* familiae overrepresented in these mice.

Statistical testing by Adonis confirms the significant differences between the 3 groups (overall $P < 0.001$). DSS treatment resulted in a significant reduction in *Prevotellaceae* (Fig. 6C; 28.8% in controls, 15.6% in the DSS group). The reduction was prevented by simultaneous administration of GHC2 (24.8%, $P < 0.01$ for variation between all groups, 1-way ANOVA). Similarly, the increase of *Deferribacteriaceae* in the DSS group was prevented by GHC2 treatment, although the variation

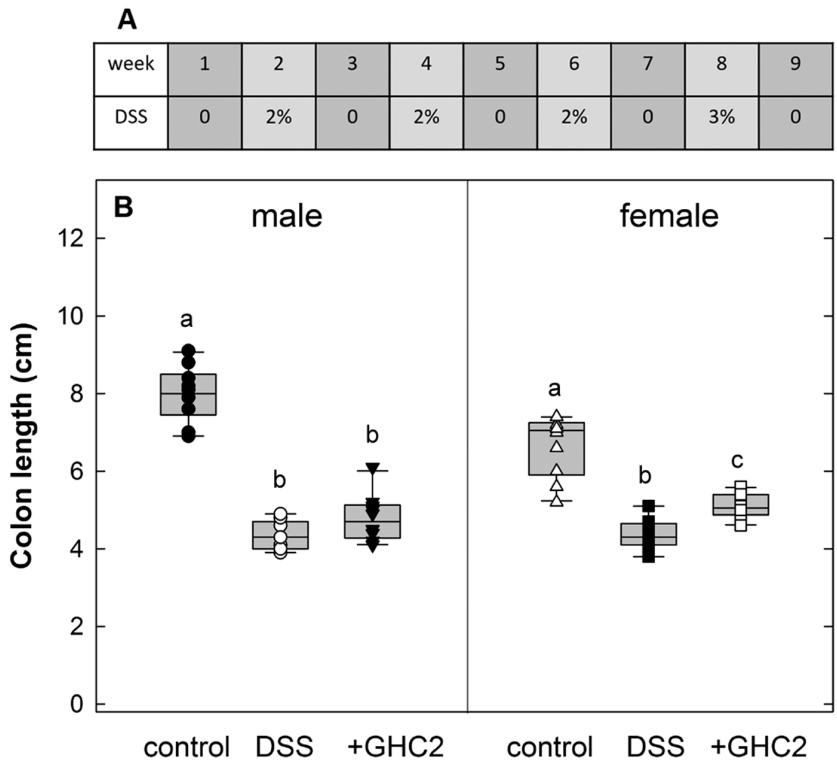

FIGURE 4. Partial protection of mice by microparticulate clinoptilolite GHC2 against colon shortening induced by chronic exposure to DSS. (A) schematic representation of the DSS-treatment regimen received by mice of the DSS and GHC2 group. Mice were exposed every other week to DSS (2% or 3% as indicated) and received regular chow (DSS) or chow fortified with 2% (wt/wt) microparticulate preparation GHC2 (+GHC2). Control mice were not challenged with DSS and received regular chow. (B) After 9 weeks the animals were killed, the colon was dissected, and its length determined. Shown are the individual values and a boxplot with the median and interquartile range (whiskers indicate the maxima and minima). The statistical comparison was done by ANOVA followed by pairwise multiple comparison with the Holm-Sidak procedure, which showed that—when compared to DSS-treated animals—GHC2 significantly ($P = 0.001$) blunted colon shortening in female animals; in male animals the difference did not reach the threshold of statistical significance ($P = 0.10$). For all groups with the same letter, the difference between the means was not statistically significant. If two groups have different letters, they were significantly different ($P < 0.05$). Males were not compared to females.

between groups was not significant ($P = 0.1$). The changes in abundance of *Lactobacillaceae*, *Porphyromonadaceae* GHC1; C *Verrucomicrobiaceae* were refractory to GHC2 treatment. Overall, a reduction of the phylum *Bacteroidetes* was observed only in the DSS group (62.2% in controls, 53.7% in the DSS group, $P < 0.05$) and not in the GHC2 group (61.9%, $P = 1$), and was mainly explained by the reduction of *Prevotellaceae* as indicated above.

DISCUSSION

The breakdown of the epithelial barrier and/or the protective mucus layer is thought to be a crucial step in the pathogenesis of human IBD.[39,40] Repeated administration of DSS to mice or rats[21] results in increased permeability, which triggers a profound inflammatory response and thus recapitulates several aspects of IBD in human subjects.[34,41,42] Compounds that adsorb toxic bacterial products are predicted to tip the balance between inflammatory damage to and regeneration of the epithelium, provided that their adsorptive capacity is large enough.[43] Therefore, in the present study, we explored 2 preparations of finely ground clinoptilolite, which differed in size but not in mineralogical or chemical composition. Our observations show that the microparticulate preparation GHC2 was more effective than the standard preparation GHC1 in remedying the DSS-induced inflammation and intestinal damage: the action of GHC1 only sufficed to blunt the induction of IL-1β and IL-6 mRNA expression, but it failed to affect the histological signs of colonic inflammation. In contrast, GHC2 reduced both the accumulation of transcripts encoding IL-1β and IL-6 and the histological damage score in a statistically significant manner. In fact, the lower efficacy of GHC1 was evidenced by the more limited decrease in IL-6 mRNA expression compared to GHC2. The efficacy of GHC2 was comparable to that of the reference compound 5-aminosalicylic acid (mesalazine). The difference between the two clinoptilolite preparations can be rationalized by considering the increase in surface area and hence in the adsorptive capacity, which is associated with a 10-fold reduction in particle size.

There is little evidence to suggest that the clinoptilolite preparations exerted their effects by any mechanism of action other than their adsorptive capacity. This conclusion is based

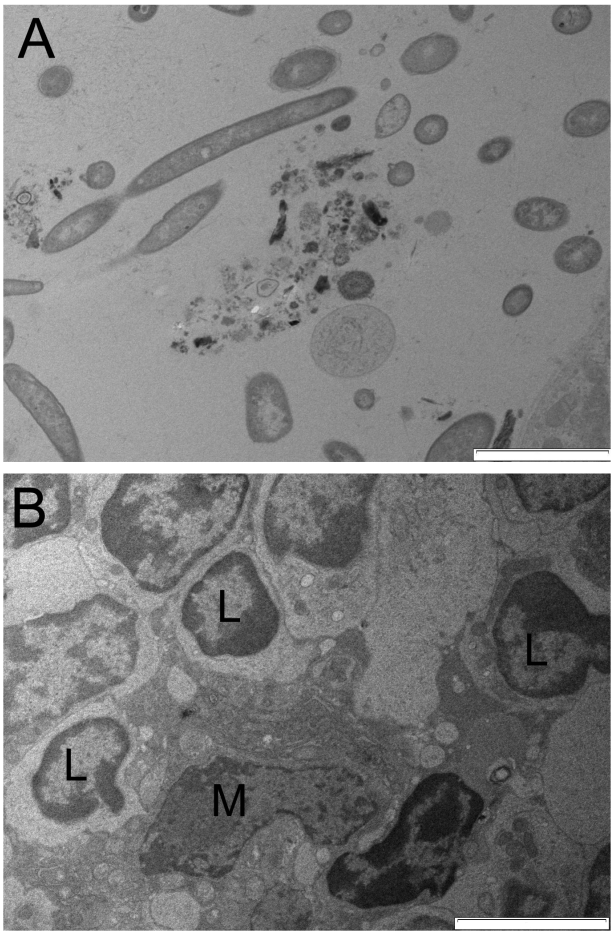

FIGURE 5. Detection of clinoptilolite particles in the gut lumen (A) but not in intestinal lymph nodes (B) by transmission electron microscopy. Samples were processed and sectioned as outlined under Materials and Methods and examined by transmission electron microscopy under 10,000-fold (A) and 3100-fold magnification (B). Panel A: clinoptilolite particles were visible in the gut lumen along with bacteria. Panel B: ultrastructure of an intestinal lymph follicle showing lymphocytes (L) and macrophages (M). Scale bars in panels A and B indicate 2 µm and 5 µm, respectively.

on the following arguments (i) We verified that the chemical purification procedure had reduced the contamination with trace elements to negligible levels. It is therefore unlikely that the anti-inflammatory actions were due to the actions of leached metals or metalloids, eg, arsenic, which can modulate the activation of neutrophils[44] and other leucocytes.[45] (ii) GHC1 and GHC2 did not differ in chemical composition but in biological action. Because identical doses of GHC1 and GHC2 were administered, this again argues against a mechanism of action that is based on the release of trace chemicals. (iii) DSS-induced colitis is known to affect the gut microbiome in a profound way.[46] This finding was recapitulated in our analysis. The effect of GHC2, however, was more subtle: DSS treatment significantly reduced the *Prevotella* phylum (*Bacteroidetes*). This was prevented by administration of GHC2. The abundance of *Firmicutes* did not change in our experiments (data not shown). A decrease in the ratio of *Bacteroidetes* over *Firmicutes* has been proposed to reflect an adverse effect on the microbiome.[47] Therefore, a restoration of *Bacteroidetes* levels could be considered a beneficial action of GHC2. However, the relationship between cause and effect is unclear: GHC2 brought about a decrease in intestinal inflammation and this may suffice to elicit changes in the microbiome. Conversely, clinoptilolite may affect the growth of intestinal bacteria[9] and/or adsorb bacterial metabolites and endotoxins,[48] which could mitigate the inflammatory response. Regardless of the underlying mechanism, it appears safe to conclude that the adsorptive property of GHC2 clinoptilolite was responsible for the beneficial effect.

Particles can induce effects by their form and size rather than by their physicochemical composition. The most conspicuous example is asbestos.[49] Dietary and other ingested microparticles have been suggested to exert actions on the immune system by their uptake via macrophages, which accumulate in Peyer's patches.[37,50] Several uptake mechanisms have been proposed, including phagocytosis by M cells, engulfment by epithelial cells, and paracellular entry.[36,37,51,52] Our experiments were specifically designed to address a possible uptake of microparticulate clinoptilolite (GHC2) through the epithelium by treating mice suffering from chronic DSS-induced colitis for a prolonged time. The findings were unequivocal: transmission electron microscopy failed to detect any clinoptilolite particles in the surface epithelium, in goblet cells, and in cells belonging to deeper layers. The examination focused on the phagocytic cells in the lymph follicles in the colon and found no clinoptilolite particles. We stress, however, that clinoptilolite particles were readily detected in the gut lumen. Thus, transmission electron microscopy was sensitive enough to detect GHC2 particles as can be expected given the high density of the crystal lattice. Liver sections also were examined to determine if GHC2 did cross the intestinal barrier to enter the systemic circulation directly via capillaries or indirectly via lymphatic vessels to eventually bind to and be phagocytosed by Kupffer cells in the liver, the resident macrophages of the liver.[53] Again, our observations did not reveal any clinoptilolite particles trapped in the liver tissue. It is obviously not possible to completely rule out any systemic availability of clinoptilolite GHC2 microparticles. However, the fact that these were absent in 58 ultrathin sections puts an upper limit on the probability for clinoptilolite microparticle entry, even if the mucosal barrier is lesioned by chronic inflammation. A recent study highlighted the role of the mucus to fend off nanoparticles.[54] The fact that clinoptilolite particles were found in the gut lumen rather than on the epithelium is consistent with these earlier observations. At the very least, our observations indicate that an inflamed gut can be exposed to clinoptilolite microparticles (GHC2) for prolonged periods without incurring a major risk for uptake and intracellular accumulation of particles. Thus, the repeated oral administration of clinoptilolite was found to be safe. Whether or not

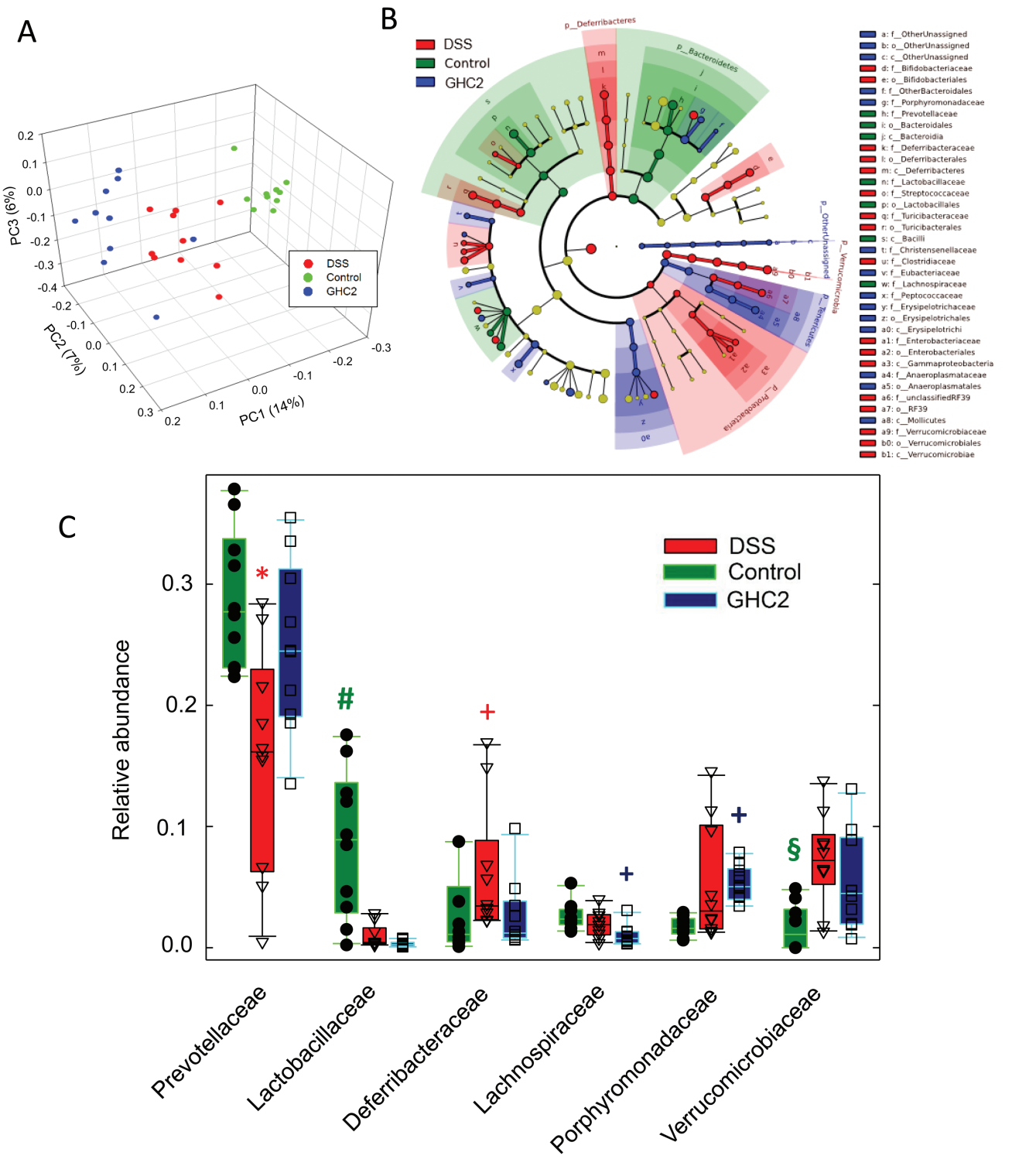

FIGURE 6. Microbiome analysis. (A) Principal component analysis (PCoA) of the microbiome composition of controls (green), DSS (red) and GHC2 (blue), based on unweighted unifrac distances. The three principal components (PC) that account most for the variation are shown (PC1 accounts for 14%, PC2 for 7%, and PC3 for 6% of total variation). Axes show the fractional value of the principal component. (B): Cladogram resulting from LEfSe analysis representing the phylogenetic tree of the taxonomic units. Coloring represents the experimental group with significant LDA score (controls—green; DSS—red; GHC2—blue; no significant score—yellow). Overall shading of branches indicates the experimental group that significantly changed in this branch. Symbol color intensity represents the effect size of individual taxa, size of the symbols is proportional to the abundance of the taxon. (C) Familiae most significantly changed by the treatment; box plots indicate median and interquartile range, whiskers denote the 95% confidence

it is an effective option for IBD treatment obviously requires further testing on additional models of the disease.

SUPPLEMENTARY DATA

Supplementary data are available at *Inflammatory Bowel Diseases* online.

ACKNOWLEDGEMENTS

The authors acknowledge J. Fendrych, I. Czucker and E. Matiasek for clinoptilolite preparation and analysis, I. Cantarero and C. Navarrete for conducting the acute DSS model and G. Siaulyte and U. Fackelmann for conducting the chronic DSS study.

Supported by GLOCK Health, Science and Research GmbH. Michael Freismuth that is the recipient of an unrestricted grant by a philanthropic foundation of Gaston H. Glock. Lukas Kenner was supported by grant FWF, P26011 and by the BM Fonds No. 15142 and the Margaretha Hehberger Stiftung No. 15142. He receives funding from the European Union's Horizon 2020 Marie Sklodowska Curie Innovative Training Network ALKATRAS under grant agreement 675712. He is head of the Core-Lab 2 of the CB-med Consortium which is funded by the FFG.

Authors' contributions

Stéphane Nizet, Eduardo Muñoz, Bernd L. Fiebich, Peter M. Abuja, Karl Kashofer, Kurt Zatloukal, Simone Tangermann, Lukas Kenner, Cornelius Tschegg, Dietmar Nagl, Laurenz Scheichl, Claudia Meisslitzer-Ruppitsch, Michael Freissmuth and Thomas Berger.

Cornelius Tschegg supervised the clinoptilolite tuff production process, Cornelius Tschegg and Laurenz Scheichl characterized clinoptilolite tuff, Eduardo Muñoz and Bernd L. Fiebich supervised the acute DSS model, Lukas Kenner and Simone Tangermann reviewed and scored the histology in a blinded fashion. Peter M. Abuja designed the chronic DSS study and experiments, performed data evaluation and interpretation of results, and contributed to writing of the manuscript; Kurt Zatloukal designed the chronic DSS study and contributed to writing of the manuscript, Karl Kashofer performed the microbiome analysis, evaluation, and interpretation of the results, Dietmar Nagl prepared and analyzed the samples in scanning electron microscopy; Stéphane Nizet, Thomas Berger, and Michael Freissmuth contributed to the design of the studies. Stéphane Nizet and Claudia Meisslitzer-Ruppitsch performed the preparation and observations in transmission electron microscopy. Stéphane Nizet and Michael Freissmuth wrote the manuscript.

REFERENCES

1. Colella C. A critical reconsideration of biomedical and veterinary applications of natural zeolites. *Clay Miner.* 2011;46:295–309.
2. Inglezakis VJ, Loizidou MD, Grigoropoulou HP. Ion exchange of Pb(2+), Cu(2+), Fe(3+), and Cr(3+) on natural clinoptilolite: selectivity determination and influence of acidity on metal uptake. *J Colloid Interface Sci*. 2003;261:49–54.
3. Sprynskyy M, Buszewski B, Terzyk AP, et al. Study of the selection mechanism of heavy metal (Pb2+, Cu2+, Ni2+, and Cd2+) adsorption on clinoptilolite. *J Colloid Interface Sci*. 2006;304:21–28.
4. Beltcheva M, Metcheva R, Popov N, et al. Modified natural clinoptilolite detoxifies small mammal's organism loaded with lead I. Lead disposition and kinetic model for lead bioaccumulation. *Biol Trace Elem Res*. 2012;147:180–188.
5. Norouzian MA, Valizadeh R, Khadem AA, et al. The effects of feeding clinoptilolite on hematology, performance, and health of newborn lambs. *Biol Trace Elem Res*. 2010;137:168–176.
6. Subramaniam MD, Kim IH. Clays as dietary supplements for swine: a review. *J Anim Sci Biotechnol*. 2015;6:38.
7. Huwig A, Freimund S, Käppeli O, et al. Mycotoxin detoxication of animal feed by different adsorbents. *Toxicol Lett*. 2001;122:179–188.
8. Katsoulos PD, Karatzia MA, Boscos C, et al. In-field evaluation of clinoptilolite feeding efficacy on the reduction of milk aflatoxin M1 concentration in dairy cattle. *J Anim Sci Technol*. 2016;58:24.
9. Prasai TP, Walsh KB, Bhattarai SP, et al. Zeolite food supplementation reduces abundance of enterobacteria. *Microbiol Res*. 2017;195:24–30.
10. Katsoulos PD, Zarogiannis S, Roubies N, et al. Effect of long-term dietary supplementation with clinoptilolite on performance and selected serum biochemical values in dairy goats. *Am J Vet Res*. 2009;70:346–352.
11. Papaioannou DS, Kyriakis SC, Papasteriadis A, et al. Effect of in-feed inclusion of a natural zeolite (clinoptilolite) on certain vitamin, macro and trace element concentrations in the blood, liver and kidney tissues of sows. *Res Vet Sci*. 2002;72:61–68.
12. Adamis Z, Tátrai E, Honma K, et al. In vitro and in vivo tests for determination of the pathogenicity of quartz, diatomaceous earth, mordenite and clinoptilolite. *Ann Occup Hyg*. 2000;44:67–74.
13. Ivkovic S, Deutsch U, Silberbach A, et al. Dietary supplementation with the tribomechanically activated zeolite clinoptilolite in immunodeficiency: effects on the immune system. *Adv Ther*. 2004;21:135–147.
14. Pavelić K, Hadzija M, Bedrica L, et al. Natural zeolite clinoptilolite: new adjuvant in anticancer therapy. *J Mol Med (Berl)*. 2001;78:708–720.
15. Papaioannou DS, Kyriakis CS, Alexopoulos C, et al. A field study on the effect of the dietary use of a clinoptilolite-rich tuff, alone or in combination with certain antimicrobials, on the health status and performance of weaned, growing and finishing pigs. *Res Vet Sci*. 2004;76:19–29.
16. Pourliotis K, Karatzia MA, Florou-Paneri P, et al. Effects of dietary inclusion of clinoptilolite in colostrum and milk of dairy calves on absorption of antibodies against *Escherichia coli* and the incidence of diarrhea. *Anim Feed Sci Technol*. 2012;172:136–140.
17. Molodecky NA, Soon IS, Rabi DM, et al. Increasing incidence and prevalence of the inflammatory bowel diseases with time, based on systematic review. *Gastroenterology*. 2012;142:46–54.
18. Ananthakrishnan AN. Epidemiology and risk factors for IBD. *Nat Rev Gastroenterol Hepatol*. 2015;12:205–217.
19. De Lange KM, Moutsianas L, Lee JC, et al. Genome-wide association study implicates immune activation of multiple integrin genes in inflammatory bowel disease. *Nat Genet*. 2017;49:256–261.
20. Ye BD, McGovern DP. Genetic variation in IBD: progress, clues to pathogenesis and possible clinical utility. *Expert Rev Clin Immunol*. 2016;12:1091–1107.
21. Okayasu I, Hatakeyama S, Yamada M, et al. A novel method in the induction of reliable experimental acute and chronic ulcerative colitis in mice. *Gastroenterology*. 1990;98:694–702.
22. Liu Z, DeSantis TZ, Andersen GL, et al. Accurate taxonomy assignments from 16S rrna sequences produced by highly parallel pyrosequencers. *Nucleic Acids Res*. 2008;36:e120.

interval; symbols indicate the relative abundance in individual animals. Differences within a familia were assessed for their statistical significance by ANOVA or Kruskal-Wallis test followed by pairwise multiple comparison with the Holm-Sidak procedure or Tukey's posthoc test, respectively: the most conspicuous differences were the DSS-induced reduction in *Prevotellaceae* (*, $P < 0.001$ vs. control and $P < 0.05$ vs. DSS+GHC2-treated animals), the abundance of *Lactobacillaceae* in control animals (#, $P < 0.05$ vs. DSS- and DSS+GHC2-treated animals), the overrepresentation of *Deferribacteraceae* in DSS-treated animals (+, $P < 0.05$ vs. control), the reduction of *Lachnospiraceae* in DSS+GHC2 treated animals (+, $P < 0.05$ vs. control), the increase in *Porphyromonadaceae* in DSS+GHC2 treated animals (+, $P < 0.05$ vs. control), and the overrepresentation of *Verrucomicrobiaceae* in DSS- and DSS+GHC2-treated animals (§, $P < 0.01$ and $P < 0.05$ for control vs. DSS- and vs. DSS+GHC2-treated animals, respectively).

23. Schmieder R, Edwards R. Fast identification and removal of sequence contamination from genomic and metagenomic datasets. *Plos One*. 2011;6:e17288.
24. Bragg L, Stone G, Imelfort M, et al. Fast, accurate error-correction of amplicon pyrosequences using acacia. *Nat Methods*. 2012;9:425–426.
25. Edgar RC. Search and clustering orders of magnitude faster than BLAST. *Bioinformatics*. 2010;26:2460–2461.
26. Caporaso JG, Kuczynski J, Stombaugh J, et al. QIIME allows analysis of high-throughput community sequencing data. *Nat Methods*. 2010;7:335–336.
27. Segata N, Izard J, Waldron L, et al. Metagenomic biomarker discovery and explanation. *Genome Biol*. 2011;12:R60.
28. Kubota M, Nakabayashi T, Matsumoto Y, et al. Selective adsorption of bacterial cells onto zeolites. *Colloids Surf B Biointerfaces*. 2008;64:88–97.
29. Hrenovic J, Ivankovic T, Tibljas D. The effect of mineral carrier composition on phosphate-accumulating bacteria immobilization. *J Hazard Mater*. 2009;166:1377–1382.
30. Söderholm JD, Peterson KH, Olaison G, et al. Epithelial permeability to proteins in the noninflamed ileum of Crohn's disease? *Gastroenterology*. 1999;117:65–72.
31. Mankertz J, Schulzke JD. Altered permeability in inflammatory bowel disease: pathophysiology and clinical implications. *Curr Opin Gastroenterol*. 2007;23:379–383.
32. Jäger S, Stange EF, Wehkamp J. Inflammatory bowel disease: an impaired barrier disease. *Langenbecks Arch Surg*. 2013;398:1–12.
33. Perše M, Cerar A. Dextran sodium sulphate colitis mouse model: traps and tricks. *J Biomed Biotechnol*. 2012;2012:718617.
34. Poritz LS, Garver KI, Green C, et al. Loss of the tight junction protein ZO-1 in dextran sulfate sodium induced colitis. *J Surg Res*. 2007;140:12–19.
35. Lamprecht M, Bogner S, Steinbauer K, et al. Effects of zeolite supplementation on parameters of intestinal barrier integrity, inflammation, redoxbiology and performance in aerobically trained subjects. *J Int Soc Sports Nutr*. 2015;12:40.
36. Becker HM, Bertschinger MM, Rogler G. Microparticles and their impact on intestinal immunity. *Dig Dis*. 2012;30(Suppl 3):47–54.
37. Carr KE, Smyth SH, McCullough MT, et al. Morphological aspects of interactions between microparticles and mammalian cells: intestinal uptake and onward movement. *Prog Histochem Cytochem*. 2012;46:185–252.
38. Hidalgo IJ, Raub TJ, Borchardt RT. Characterization of the human colon carcinoma cell line (caco-2) as a model system for intestinal epithelial permeability. *Gastroenterology*. 1989;96:736–749.
39. Hollander D, Vadheim CM, Brettholz E, et al. Increased intestinal permeability in patients with Crohn's disease and their relatives. A possible etiologic factor. *Ann Intern Med*. 1986;105:883–885.
40. D'Incà R, Annese V, di Leo V, et al. Increased intestinal permeability and NOD2 variants in familial and sporadic Crohn's disease. *Aliment Pharmacol Ther*. 2006;23:1455–1461.
41. Vetrano S, Rescigno M, Cera MR, et al. Unique role of junctional adhesion molecule-a in maintaining mucosal homeostasis in inflammatory bowel disease. *Gastroenterology*. 2008;135:173–184.
42. Johansson ME, Gustafsson JK, Holmén-Larsson J, et al. Bacteria penetrate the normally impenetrable inner colon mucus layer in both murine colitis models and patients with ulcerative colitis. *Gut*. 2014;63:281–291.
43. Gardiner KR, Anderson NH, McCaigue MD, et al. Adsorbents as antiendotoxin agents in experimental colitis. *Gut*. 1993;34:51–55.
44. Binet F, Girard D. Novel human neutrophil agonistic properties of arsenic trioxide: involvement of p38 mitogen-activated protein kinase and/or c-jun NH2-terminal MAPK but not extracellular signal-regulated kinases-1/2. *J Leukoc Biol*. 2008;84:1613–1622.
45. Binet F, Antoine F, Girard D. Interaction between arsenic trioxide and human primary cells: emphasis on human cells of myeloid origin. *Inflamm Allergy Drug Targets*. 2009;8:21–27.
46. Schwab C, Berry D, Rauch I, et al. Longitudinal study of murine microbiota activity and interactions with the host during acute inflammation and recovery. *Isme J*. 2014;8:1101–1114.
47. Berry D, Kuzyk O, Rauch I, et al. Intestinal microbiota signatures associated with inflammation history in mice experiencing recurring colitis. *Front Microbiol*. 2015;6:1408.
48. Wu QJ, Zhou YM, Wu YN et al. The effects of natural and modified clinoptilolite on intestinal barrier function and immune response to LPS in broiler chickens. *Vet Immunol Immunopathol*. 2013;153:70–76.
49. Stanton MF, Layard M, Tegeris A, et al. Relation of particle dimension to carcinogenicity in amphibole asbestoses and other fibrous minerals. *J Natl Cancer Inst*. 1981;67:965–975.
50. Powell JJ, Faria N, Thomas-McKay E, et al. Origin and fate of dietary nanoparticles and microparticles in the gastrointestinal tract. *J Autoimmun*. 2010;34:J226–J233.
51. Hazzard RA, Hodges GM, Scott JD, et al. Early intestinal microparticle uptake in the rat. *J Anat*. 1996;189(Pt 2):265–271.
52. Damgé C, Aprahamian M, Marchais H, et al. Intestinal absorption of PLAGA microspheres in the rat. *J Anat*. 1996;189(Pt 3):491–501.
53. Sadauskas E, Wallin H, Stoltenberg M, et al. Kupffer cells are central in the removal of nanoparticles from the organism. *Part Fibre Toxicol*. 2007;4:10.
54. Sinnecker H, Krause T, Koelling S, et al. The gut wall provides an effective barrier against nanoparticle uptake. *Beilstein J Nanotechnol*. 2014;5:2092–2101.